Journal of Alloys and Compounds 936 (2023) 168165

Contents lists available at ScienceDirect

Journal of Alloys and Compounds

journal homepage: www.elsevier.com/locate/jalcom

Research article

Shear transformation zones and serrated flow dynamics of metallic glasses revealed by nanoindentation

Yuexin Chu [a,b], Guishen Zhou [a], Shaoshan Wan [a], Yue Zhang [a,*], Fuyu Dong [a,*], Xiaoguang Yuan [a], Binbin Wang [c], Liangshun Luo [c], Yanqing Su [c], Weidong Li [d], Peter K. Liaw [d]

[a] School of Materials Science and Engineering, Shenyang University of Technology, Shenyang, China
[b] School of Materials Science and Engineering, Northeastern University, Shenyang, China
[c] School of Materials Science and Engineering, Harbin Institute of Technology, Harbin, China
[d] The Department of Materials Science and Engineering, University of Tennessee, Knoxville, TN, USA

ARTICLE INFO

Article history:
Received 6 September 2022
Received in revised form 5 November 2022
Accepted 21 November 2022
Available online 24 November 2022

Keywords:
Metallic glass
Nanoindentation
Shear transformation zone
Statistical analysis
Serrations

ABSTRACT

The relationship between shear transformation zones (STZs) and serrated flow dynamics of Co-, Fe-, Zr-, La- and Al-based metallic glasses (MGs) with different plasticity were analyzed by nanoindentation. The serrated flow dynamic behaviors were analyzed using statistical analysis of shear stress drops, $\Delta\tau$. The STZ size was estimated via the nanoindentation creep method based on the cooperative shear model. Examination of two distinct types of serrated flow dynamics were performed. For MGs (e.g., Al- or Zr-based) where STZs could be easily activated or at low loading rates, shear stress exhibited a decreasing trend and followed a power-law distribution, which was an indicator of a self-organized critical (SOC) state in the dynamics. In contrast, a Gaussian law distribution was found for STZs in hard MGs (e.g., La-, Co-, and Fe-based) or at high loading rate. In the case of Gaussian distribution case, serrated flow dynamics were in a chaotic state, which indicated that STZ aggregation reduced the stresses required for plastic deformation.

1. Introduction

Combined with glass structures and metal-bond characteristics, metallic glasses (MGs) exhibit many excellent mechanical properties, such as high strength, great elasticity, wear resistance, and corrosion resistance [1,2]. MGs show a wide range of application prospects in aerospace, precision machinery, military weapons, and other high-tech fields [3,4]. However, when subjected to external stresses, the disordered atomic structure of an MG cannot produce plastic deformation through dislocation movement as can crystalline materials [5]. The overall plasticity or toughness are very limited for many MGs at temperatures far below their glass transition temperature, which greatly limits their applications [1,6,7]. Therefore, unraveling the plastic deformation mechanism [7–10] in parallel with pragmatic efforts to develop an effective plasticizing process method [11–13] has been the subject of extensive research in past decades and still attracts considerable interest.

The exact nature of local atomic movement in deforming MGs has not been fully resolved, although there is general a consensus that the fundamental unit process underlying deformation must be a local rearrangement of atoms that can accommodate shear strains [14]. At room temperature, the shear band is the most important feature of deformation, which is closely related to the mechanical behavior of MGs, such as yield, plasticity, and fracture [15–17]. Under restricted loading conditions, such as compression [18] and cold-rolling [19], the restriction of the normal stress or geometrical shape on the expansion and movement of shear bands forces them to multiply and intersect with one another. This cooperative shear motion effectively dissipates the external work and results in a certain degree of plastic deformation in MGs. Owing to the pioneering work by Argon [20], the evolutional processes of shear bands are known to associate with the shear transformation zone (STZ), which spontaneously and cooperatively reorganizes under the action of shear stress. In this deformation process, the material transitions from a high energy state to a low energy state, and many free volumes are excited. However, unlike the grain-boundary and dislocation of crystalline materials, the morphology of STZs cannot be observed directly by electron and light microscopies [2,21]. Nonetheless, considering the fact that plastic deformation in MGs is accomplished through the activation of the deformation unit existing

* Corresponding authors.
E-mail addresses: yuezhang@sut.edu.cn (Y. Zhang), dongfuyu2002@163.com (F. Dong).

https://doi.org/10.1016/j.jallcom.2022.168165
0925-8388/

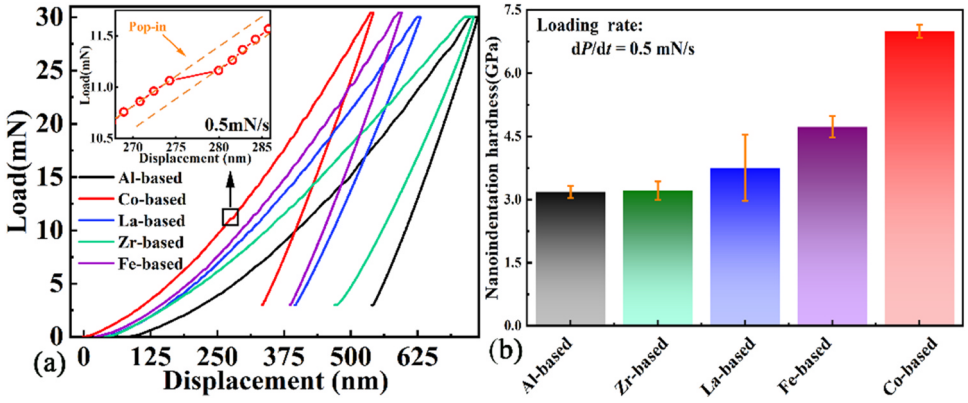

Fig. 1. Load-displacement (*P-h*) curves (a) and nanoindentation hardness (b) of Co-, Fe-, La-, Zr-, and Al-based MGs.

in its own structure [11,22], the heterogeneous microstructure of MGs is the key to understanding their deformation behavior [23–26].

The macroscopic plastic flow in an avalanche-like manner of the MG is manifested as a serrated flow behavior on the stress-strain curve [27]. Intermittent shear avalanche behavior [28] is induced when the STZ interacts with each other, which corresponds to serrated flow during deformation [27,29,30]. Avalanche dynamics and deformation structure have been shown to be important concepts for the description of the MG plasticity [31]. Recently, research on flow behavior of MG has been attracting increasing attention regarding increased understanding of their plasticity mechanism [11,32–34]. Li et al. [35] have shown that avalanche events in the plastic flow of bulk MG agree with the mean-field theory and have seismic-like size dynamics. Sun et al. [36] have studied the macroscopic serrated rheological behavior of amorphous alloys from the perspective of complex dynamic evolution by compression tests of eight different MGs and found that serrated flow behavior in ductile amorphous alloys is in a self-organized critical (SOC) state. The SOC behavior is characterized by the continuous propagation of deformation bands near the upper strain rate boundary of plastic instability. At lower strain rates, successive formation of distinct and adjacent deformation bands is described as chaotic behavior [37]. Krisponeit et al. [38] have proposed an experimental method to provide evidence for SOC formed by the interactions of the STZs of amorphous alloys. The study of the relationship between STZ and SOC behavior of amorphous rheology is indispensable for revealing inhomogeneous deformation and provides a theoretical basis for finding several plasticizing methods.

Accordingly, in this study, nanoindentation was used to investigate the flow unit and dynamic behavior of MGs, relying on the high spatial and temporal resolution of instrumented nanoindentation. The *P-h* curves of MGs have visible serration flows (pop-ins) under nanoindentation [39–41]. Based on the cooperative shear model (CSM) theory [21,42], the nanoindentation creep method [11,43–45] was used to extract the STZ parameters of MGs at the holding stage. Zirconium, aluminum, cobalt, lanthanum, and iron (Zr, Al, Co, La, and Fe, respectively)-based MGs were chosen for examination, given they possess different mechanical properties, such as hardness, Poisson's ratio, and plasticity. Statistical analysis of the shear strain mutation of each serration flow was conducted to gain a better understanding of the dynamic behavior during the deformation process. Finally, the relationship between SOC behavior and flow units of the MGs were examined.

2. Experimental

Master alloy ingots with nominal compositions of $Zr_{64}Cu_{22}Al_{12}$, $Al_{85}Y_{5.5}Fe_{2.5}Co_2Ni_5$, $Co_{39}Nb_{31.2}Fe_{7.8}Si_6P_{16}$, $La_{70}Ni_{15}Al_{15}$, and $Fe_{78}Si_9B_{13}$ were obtained by melting high-purity metals (≥ 99.9% weight percent, wt%) in a water-cooled copper crucible in argon (Ar) atmosphere. Ingots were remelted five times, to ensure sample consistency and chemical homogeneity, and followed by melt spinning to form an amorphous ribbon. Structural analyses were conducted, using X-ray diffraction (XRD, Shimadzu XRD 7000) with Cu-K_α radiation, scanning from 20° to 100° at a speed of 5°/min.

Nanoindentation testing was performed at room temperature employing an Agilent Nano Indenter G200 (Agilent Technologies, Inc., Santa Clara, CA, USA) with a Berkovich diamond indenter. The displacement and load resolution of the machine were < 0.01 nm and 50 nN, respectively. Prior to testing, the instrument was calibrated, using standard fused silicon. In order to eliminate the thermal effect, the thermal drift correction of machine was kept below 0.05 nm/s in the indentation process. Amorphous ribbons were cut into 6 × 6 × 0.1 mm^3 samples, with one ribbon plane mechanically polished to a mirror surface. All nanoindentation experiments were loaded to 30 mN at a 0.5 mN/s loading rate under a load-control mode. The maximum load was held constant for 10 s before unloading to 10% of the maximum load at the same rate as the loading rate. The experimental data were repeated at least six times to ensure data accuracy. To reduce the effects of thermal drift [46,47] and to exclude the long time creep deformation effect, a reasonable dwell period of 10 s for the creep stage of nanoindentation is selected, because which is usually adopted in nanoindentation for the materials under the indenter to reach a steady mechanical state [48].

3. Experimental results

3.1. Nanoindentation deformation behavior

The complete load-displacement (*P-h*) curves of nanoindentations for Co-, Fe-, La-, Zr-, and Al-based MGs showed that a prominent feature of the load-displacement curve was intermittent plastic deformation during the loading phase [Fig. 1(a) and inset]. This phenomenon is called "serration flow behavior" or "pop-in" events [9,15,49]. It was found here that serration flow was affected by MG composition, as each curve had different numbers and jump widths of pop-ins. To clearly distinguish each curve, the starting point of each curve was translated horizontally.

From the above results, the following phenomena were observed: (1) At the early stage (about the first 10 s of loading), the *P-h* curves had no pop-in events, which indicated that deformation was purely elastic prior to the first serration (Fig. 1a) [45]. At the same loading rate, the width of the serration at different pressing depths are not identical. For the serration with a smaller width, plastic strain was dissipated by a single shear band, resulting in a smaller displacement mutation [16–18]. For the serration with a greater width, the newly formed shear band interacted with the former shear band before yielding, causing two or even multiple shear bands to move simultaneously [16–18]. In this situation, each serration acted in response to multiple shear bands to dissipate the plastic strain, thereby forming many larger sized serrations [16–18]. Further details of serrated flow behaviors were discussed below. (2) The serration flow behavior was closely related to various internal factors, such as the composition and ductility of the sample. When these factors changed, the size of the serration, intermittent time, and other characteristics also changed significantly. The serration phenomenon was also closely related to MG mechanical properties, such as hardness. According to nanoindentation hardness (Fig. 1b), the 5 samples were divided into hard and soft MGs. Hard MGs, such as Fe- and Co-based MGs, had smaller indentation depths at the maximum load (Fig. 1a) and larger hardness (Fig. 1b).

3.2. The serration flow behavior reflected on shear stress-displacement (τ-h) curves

In nanoindentation, the relationship between the shear stress, τ, and the nanoindentation hardness, H, is [50].

$$3\sqrt{3}\,\tau \approx H. \tag{1}$$

According to the indentation depth measurement method proposed by Oliver and Pharr [51], for an ideal Berovich indenter, the nanoindentation hardness, H, has the following relationship with the contact depth, h_c, as

$$H = \frac{P}{24.56 \times h_c^2}, \tag{2}$$

where the contact depth, h_c, is obtained from the data in the load-displacement curve and

$$h_c = h - \varepsilon \times P/S, \tag{3}$$

where ε is 0.75 and S the material stiffness determined by fitting 0–25% of the top of the unloading curve, using least squares. From the above three Eqs. 1–3, the magnitude of the shear stress was derived as

$$\tau = \frac{P}{24.56 \times 3\sqrt{3}\,(h - \varepsilon \times P/S)^2}. \tag{4}$$

The amount of stress versus displacement for samples of Co-, Fe-, Zr-, La-, and Al-based MGs are shown in Fig. 2. The following phenomena were observed:

(1) The serrated flow behavior not only occurred in load-displacement (*P-h*) curves but also in shear stress-depth (τ-h) curves (Figs. 2a-2c). There was a corresponding relationship between the curve of loads versus displacement and shear stress versus displacement (Fig. 2d). When the serrated flow behavior phenomenon occurred, the corresponding shear stress had a maximum value, and the moment that the maximum occurred indicates the transition from elasticity to plasticity. Statistical analysis of the yield strength for the onset of plastic deformation [52] was equivalent to the statistical analysis of maximum stress. The maximum shear stress, τ_{max}, was the shear stress at the transition from elasticity to plasticity and, thus, could be readily identified as the start of each serration event. (2) Clearly, the serration flow had a strong dependence on the loading rate, which has been widely reported [39,49,53,54]. A closer inspection of serrated flow in shear stress-depth (τ-h) curves revealed that the stress drop magnitudes decreased with loading rate. In the case of low loading rate (Fig. 2a and inset), more and larger stress drop were produced. In the case of high loading rates (Fig. 2b and inset), many small serrations appeared and each saw tooth appeared in a certain load range. When the loading rate was increased to 10 mN/s (Fig. 2c and inset), a smooth curve was obtained. As the strain rate increased, the serration flow behavior gradually weakened and, at a certain critical strain rate, serration rheological behavior completely disappeared. Furthermore, the intermittent-to-smooth transition indicated that the serration rheology had typical dynamic characteristics [36,55]. Schuh et al. [55] have suggested that the flow unit involved in the deformation process is similar to the defects involved in deformation of crystalline materials. In the deformation process, the accumulation of energy is required to achieve the activation, linkage, and organization of the flow unit. When the energy exceeds the barrier required for flow unit activation, the energy is released in the form of kinetic energy, which is reflected in the formation of serration flow on the stress-depth curve. For the high loading rate, the condition for generating serrations were easy to achieve, which made it impossible to have enough time to completely form serration. (3) The serration shear stress curves also showed the indentation size effect (Fig. 2a-c). The indentation-size effect (ISE) was manifested as an increase in hardness (or shear stress, $\tau = 3\sqrt{3}H$) with decreased impression size [56], and this phenomenon was clearly observed at the initial stage for indentation depths up to ~ 150 nm (termed a “strong size effect” stage). However, once the penetration depth exceeded this value, the shear stress oscillated over a narrow range (termed the “weak size effect” stage). In other words, as the indentation deepened, the ISE gradually weakened. This phenomenon suggested that the ISE was minimal in the weak size effect stage. For the initial stages of loading, the highly stressed volume beneath the indenter was probably too small to have a sufficient population of STZs, but deep indentations produced a large volume of deformation and thus, higher activities of STZs [45,57]. When the shear stress tended to be stable, the activated quantity of STZs had reached saturation. (4) The starting and end positions of pop-in events were identified through the valley and peak positions of the curves. Sudden shear stress drops ($\Delta\tau$) were seen as serration sizes and represented by the difference between the peak and valley values [Fig. 2(a) and (b)]. The shear stress drops from each serration was not the same, compared to the adjacent serration. In fact, serration behavior did not have a characteristic length or time scale.

Subsequently, oscillations with much higher frequencies but smaller amplitudes due to machine noises were also observed in samples at a load rate of 0.5 mN/s (Fig. 2b). During the experiment at a lower load rate, the noise/vibrations of the experimental equipment can also cause jagged fluctuations on the shear stress-displacement curve[58]. These noises are not considered in subsequent analysis[34]. The noise serration size of the loading stage is simar to that of the holding stage, which has been proposed in our previous work [11]. So the background noise of serration events were removed by the noise analysis for 10 s holding stage.

3.3. Dynamic behavior of serrations

The deformation of amorphous alloys involves interactions between atomic-scale deformation units and is an intermittent plastic flow event, which is typical of complex dynamic system [36]. Statistical analysis of this irregular intermittent displacement is an effective method for detecting serrated flow dynamic characteristics and better understand the MG deformation mechanism. The statistical object examined here was shear stress drop. Before statistical calculations, shear stress drops of serrations were normalized to

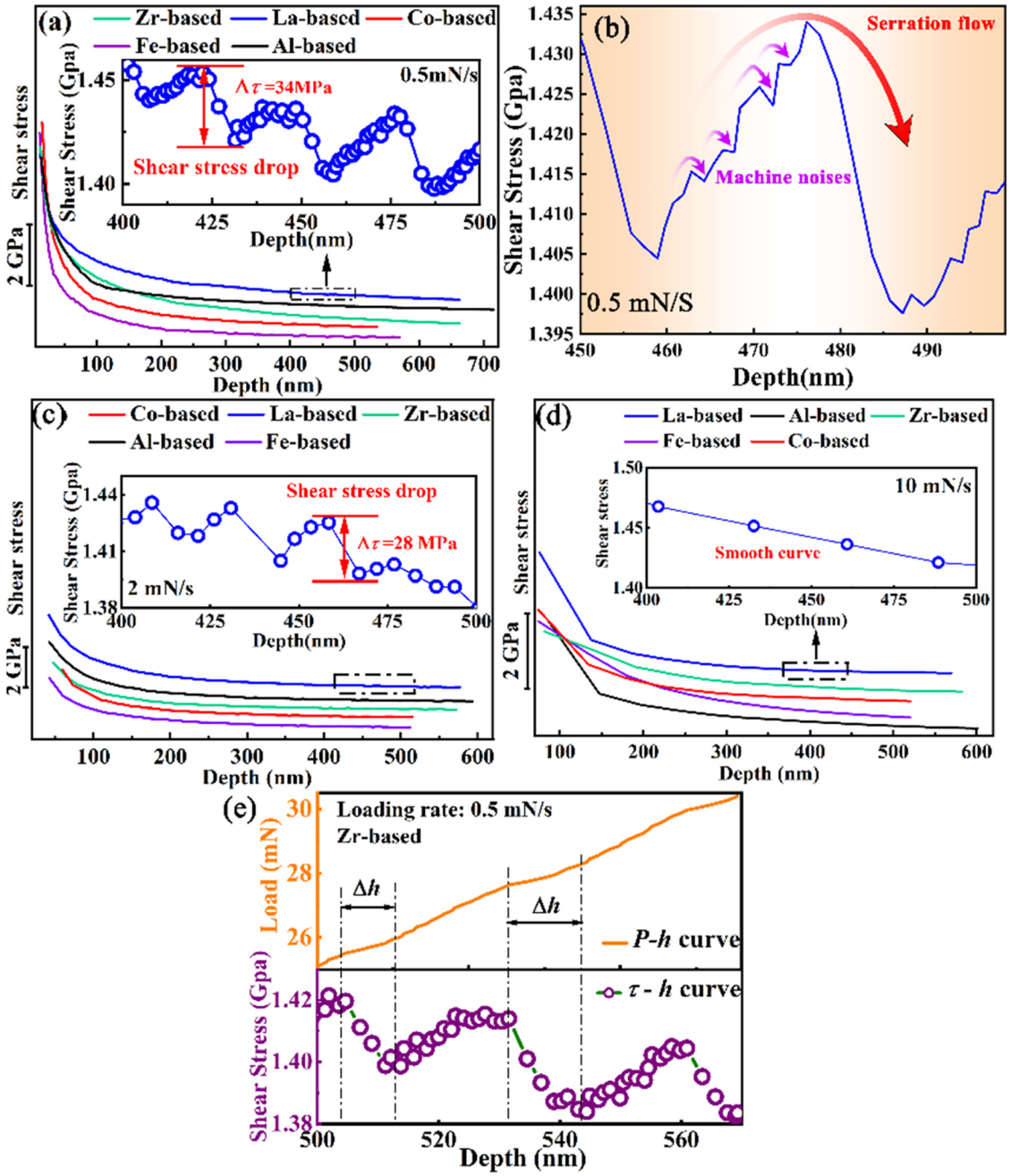

Fig. 2. Serration shear stress, τ, vs. depth, h, curves obtained at 0.5, 2, and 10 mN/s (a, c, d, respectively). Insets in Fig. 2(a, c, d) show enlarged serrated flow patterns and stress drops. Fig (b) shows machine noises at a load rate of 0.5 mN/s. Curves of serration bursts versus displacement and corresponding serration shear stress versus displacement (e).

eliminate statistical errors, which generated the normalization serration size [34,59]. The shear stress drop, $\Delta\tau$, was normalized via $S = \Delta\tau/\tau$ [34], where τ is the shear stress at pop-in occurrence, resulting in counts, $N(S)$, of normalized stress drops at different loading rates (Fig. 3).

At a low loading rate, the counts of normalized stress drops clearly showed a power law downward trend for each alloy system (Fig. 3a). With increasing the loading rate, the counts of the normalized stress drop in hard MGs presented a Gaussian distribution (Fig. 3b). This transformation phenomenon first occurred in the hard MGs (i.e., Co and Fe-based). When the strain rate increased to 2 mN/s, all samples exhibited Gaussian distributions (Fig. 3c). Generally, the counts of normalized stress drop during nanoindentation deformation suggested a chaotic dynamic state with a Gaussian-like distribution [30,36,59,60] and an SOC dynamic state with a power law distribution of serrations [34]. Thus, the dynamic behavior of serrated flow was closely related to alloy composition and loading rate.

3.4. Characterization of the STZ size

The serrated flow phenomenon in MG plastic deformation is closely related to the formation and expansion of shear bands [15,61,62]. Considering the structure of MGs, the MGs cannot activate the shear bands by the crystal defects. The plastic deformation was formed by the deformation units (such as, the STZs) [20]. However, the relationship between the STZ size and dynamic behavior remained unclear. Therefore, it was necessary to calculate the STZ size under nanoindentation.

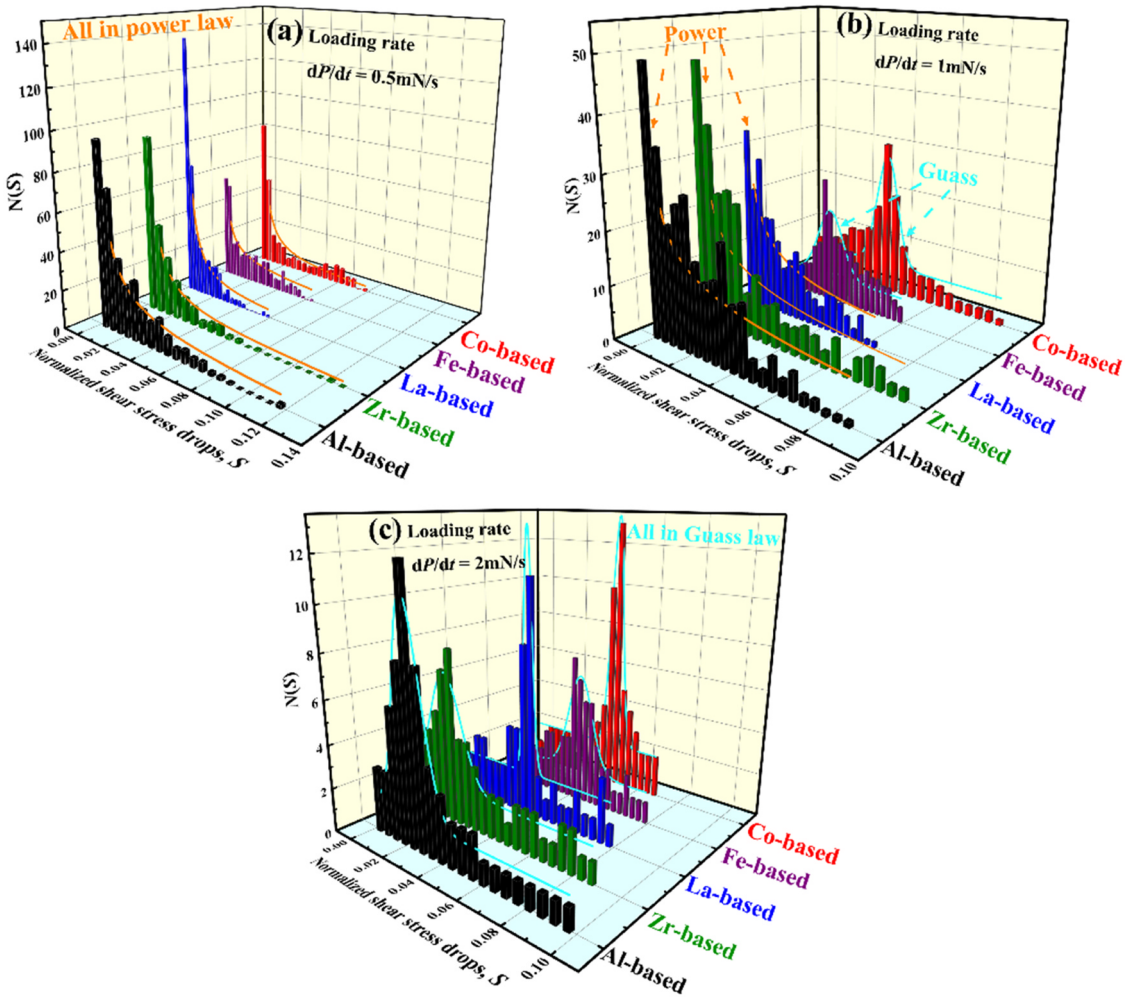

Fig. 3. Counts of normalized stress drops, $N(S)$, versus normalized stress drops, S, at loading rates of 0.5, 1, and 2 mN/s (a-c, respectively) for Al-, Zr-, La-, Fe-, and Co-based metallic glasses.

STZ is not a structural defect of MGs, but it is a basic carrier of the plastic flow. This feature is different from dislocations, which are based on both the carrier of crystal plastic rheology and static structural defects in crystals. Consequently, the STZ cannot be found from an atomic image of an amorphous solid before deformation [6,20,63,64]. Molecular dynamics simulations are commonly used to analyze STZs [65–68], but this method is more suitable for binary alloy systems. In recent years, based on the CSM theory, the nanoindentation method has been found to effectively characterize the relevant parameters of the STZ of amorphous alloys [43,52,69–71]. Pan et al. have used the nanoindentation method with different loading rates to quantitatively calculate the STZ volume of MGs [69]. The STZ volume was described as a function of Eq. (5), as.

$$\Omega = \frac{kT}{(G\gamma_c^2)}\frac{1}{6R_0\xi}\frac{1}{m\left(\frac{\tau}{\tau_c}\right)\left(1-\frac{\tau}{\tau_c}\right)^{1/2}}, \tag{5}$$

where k is the Boltzmann constant, T the temperature, m the strain-rate sensitivity exponent, $\gamma_C \approx 0.0267$, the critical shear strain, G, is the shear modulus has a weak temperature dependency for MGs [42], τ is the critical shear strength, τ_c is the critical shear stress at 0 K, $R_0 \approx 1/4$ is a constant and ξ is the correction coefficient caused by matrix binding around the internal flow unit, which was equal to 3. For nanoindentation experiments, hardness$H \approx 3\sigma_y = 3\sqrt{3}\,\tau_y$. Therefore, Eq. 5 was rewritten as

$$\Omega = \frac{\mathrm{kT}}{\frac{2R_0\xi}{\sqrt{3}}\cdot\frac{G\gamma_C^2}{\tau_c}\left(1-\frac{\tau}{\tau_c}\right)^{1/2}mH}. \tag{6}$$

The value of $\tau_c/G = 0.036$[42] and the value of τ/τ_c was estimated using the constitutive equation [42]:

$$\tau/G = \gamma_{C0} - \gamma_{C1}(T/T_g)^n, \tag{7}$$

where $\gamma_{C0} = 0.036$, $\gamma_{C1} = 0.016$, $n = 0.62$ and T_g is the glass transition temperature.

Thus, when calculating the STZ volume, the most important parameter was the strain-rate sensitivity exponent, m, which was obtained by designed creep experiments.

When the strain and temperature were determined, the relationship between the hardness (or stress) and strain rate was

$$H_{\varepsilon,t} = C_1(\dot{\varepsilon})^m, \tag{8}$$

where $H_{\varepsilon,t}$ is the hardness, C_1 the constant at same stressed state, $\dot{\varepsilon}$ the strain rate, and m the strain rate sensitivity exponent. From Eq. 8, the strain rate sensitivity exponent was obtained via establishing the relationship between the hardness and strain rate.

During the nanoindentation process, the strain rate was described as

$$\dot{\varepsilon} = \frac{\dot{h}}{h} = \frac{\mathrm{d}h/\mathrm{d}t}{h}, \tag{9}$$

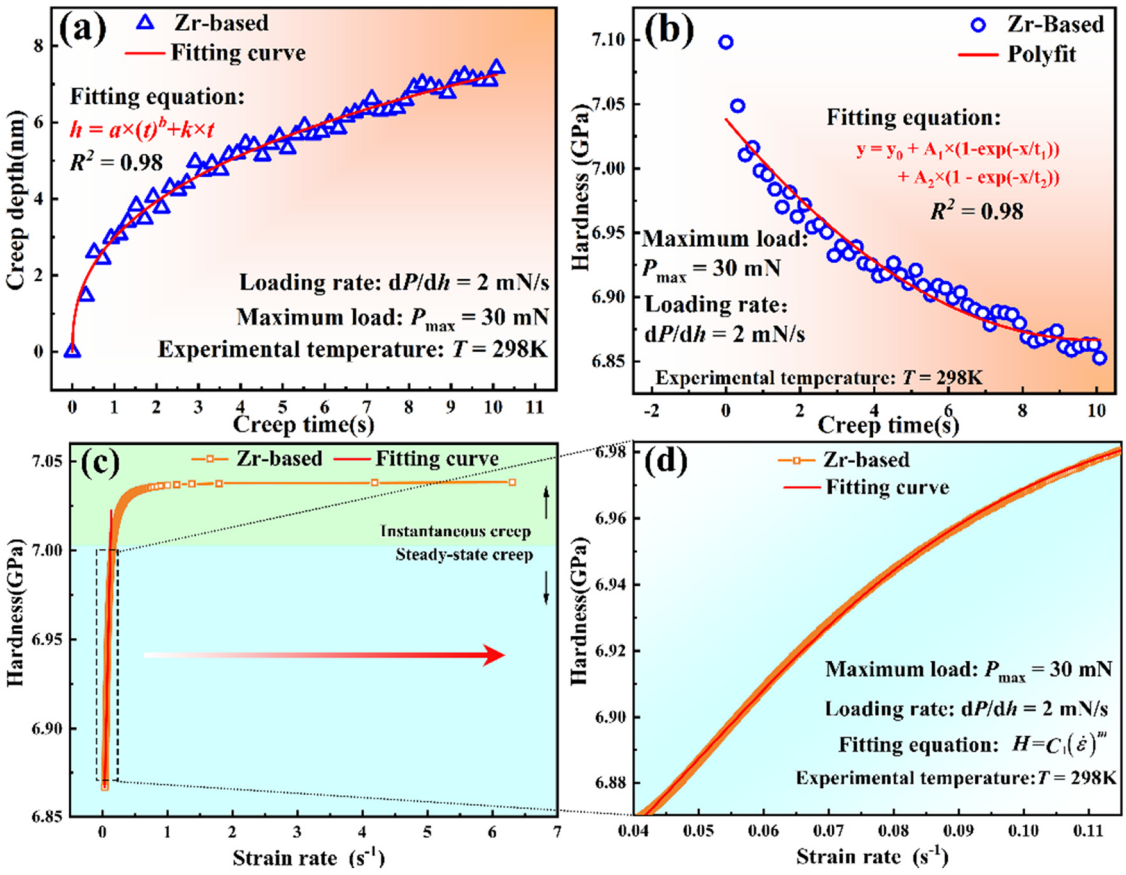

Fig. 4. Creep depth-time curve (a), hardness-creep time curve (b), and hardness-strain rate curve (c) and (d) of Zr-based at a loading rate of 2 mN/s.

where h is the displacement in the creep stage, t is the corresponding creep time, and dh/dt is the creep displacement speed. The empirical equation, $h(t) = at^b + kt$ (where a, b, and k are fitting constants), was used to fit the time-displacement data of the creep stage (Fig. 4a). After fitting, the displacement speed was obtained by derivative of the fitting curve. Creep hardness was calculated from Eqs. 2 and 3, as.

$$H = \frac{P}{24.56 \times (h - \varepsilon \times P/S)^2}, \tag{10}$$

where h is the displacement, P is the load, ε at 0.75, and S the material stiffness determined by fitting 0–25% of the top of the unloading curve using least squares. The variation of creep hardness with time showed the uniformly distributed creep time-hardness data by fitting the hardness data with two polynomial terms (Fig. 4b). The correlation between the hardness and strain rate during the holding stage showed that, m was obtained by linearly fitting part of the steady-state creep (Fig. 4c).

Results of the STZ volume, Ω, clearly showed that, with increasing the loading rate, the STZ volumes of the Co-based MG was unaffected by the loading rate (Fig. 5a). The STZ volume of Fe and La-based MGs approached their maximum at loading rates of 1 and 2 mN/s, respectively, and subsequently decreased (Figs. 5b and 5c, respectively). The STZ volume of Zr and Al-based MGs significantly decreased with increasing the loading rate (Figs. 5d and 5e, respectively). According to the experimental results of Fig. 3 as a standard to distinguish between SOC dynamic state and chaotic dynamic state with two states. Generally, the counts of normalized stress drop during nanoindentation deformation suggested a chaotic dynamic state with a Gaussian-like distribution [30,36,59,60] and an SOC dynamic state with a power law distribution of serrations [34]. In addition, the dynamic behavior of serrated flow was closely related to alloy composition and loading rate. The greater the rate, the more inclined to go into the chaotic dynamic state. Because the sample enters the chaotic dynamic state when the loading rate is 2 mN/s, samples with a load rate of 10 mN/s also thought it entered the chaotic dynamic state. Furthermore, MGs that were prone to a chaotic state in serrated flow dynamics had small STZ volumes. MGs was prone to the SOC state had large STZ volumes. Combined with the results of the shear stress (Fig. 2), the shear stress of soft MGs was relatively small when pop-ins occurred, which indicated that the internal STZ was easily activated. With the increasing difficulty of the STZ activation, the chaotic state of serrated dynamics was more easily formed. However, the relationship between the dynamic behavior, especially in the SOC state, and STZ was difficult to identify, which meant that it was incomplete for establishing the STZ volume and serrated dynamic behavior by simple statistical analysis. Therefore, other models and statistical methods were used to further discuss the dynamic behavior of the serrated flow.

4. Discussion

The serrated flow during plastic deformation of ductile MGs showed an SOC dynamic state. SOC is a theoretical concept that can explain how complexity arises [36,72]. Here, the quantitative analysis of shear stress drops by ergodic processing was introduced to understand the SOC state of serrated flow. This approach provided new insights into the underlying mechanisms of MG plastic deformation. The cumulative probability distribution, $P(>S)$, of the normalized serration size was calculated (Fig. 6).

The distribution of serration size was clearly seen to be divided into two parts. The first part contained a large number of small shear stress drops with a higher probability of occurrence, with the distribution of this part obeying the power law relationship. The second

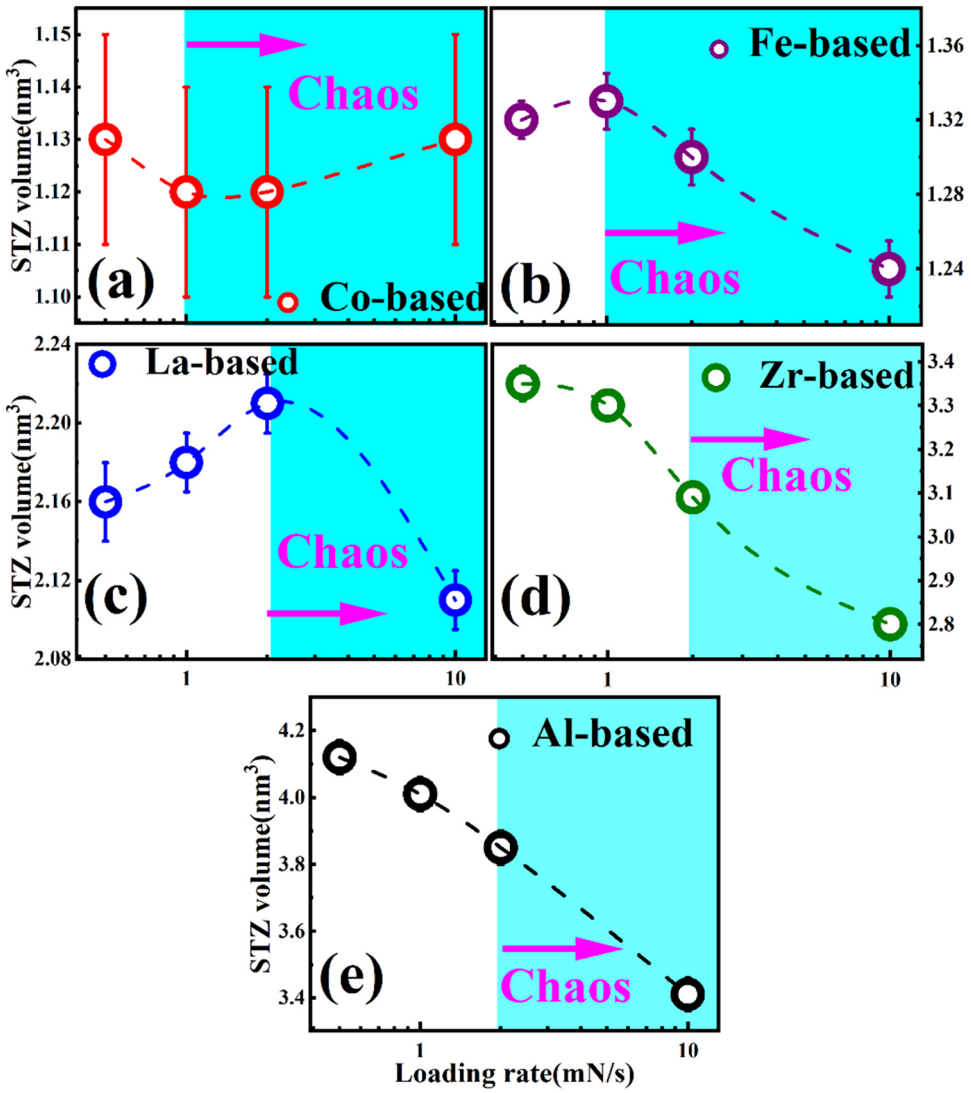

Fig. 5. Results of STZ volumes for Co-, Fe-, La-, Zr-, and Al-based MGs (a-e, respectively).

part contained a small number of large shear stress drops with an exponential distribution. The cumulative probability distribution was fitted using the following empirical formula [73], as

$$P(>S) = AS^{-\beta}\exp[-(S/S_c)^2] \quad (5)$$

where A is a normalization constant, β a scaling exponent, and S_C the cutoff value of the serration size. The fitting parameters β and S_C were the key parameters for describing the shear avalanche behavior of amorphous alloys in nanoindentation experiments [34]. The cumulative probability of serration size obeyed the power distribution, but it also showed an exponential decay when it was larger than the cutoff value. The cumulative distribution of stress drops, as observed from Eq. 5, must have a power law relationship before the cutoff value, i.e., S_c, and the subsequent exponential term the dominant contribution. Different MGs have various cutoff values for S_C (Fig. 6).

When stress was applied, the motion of unit flows in the MG made the atomic cluster transform cooperatively and then formed an STZ [42]. In the nanoindentation experiment, the load when the displacement burst event occurs slightly increased (Fig. 2d), and the slight increase in load in this shear stress drop event corresponded to activation and connection of the STZ. When the load was close to maximum, due to interactions of elastic stress fields between adjacent collaborative STZ, the expanded STZ was blocked [34]. In contrast, the increased STZ also caused greater internal stress concentration, which made plastic deformation tend to evolve into a SOC state [74]. Whatever the larger STZ volume was, the SOC behavior became more severe (Fig. 7). Meantime, the cut-off value was used to quantitatively characterize the intensity of SOC phenomena at various STZ volumes. The cut off value decreased from 0.047 ± 0.001–0.020 ± 0.001 with increasing STZ volume, from 1.13 ± 0.12–4.12 ± 0.21 nm^3 which reflected that STZ activation facilitated SOC formation.

As for the increase of loading rate, the STZ activation will become much more difficult, and the formation of shear bands is conducted by the cooperative rearrangement of relatively large STZs. It will lead to the suppressed deformation mode transition, and delay the formation of shear bands. Schuh et al. [6] have studied nanoindentation behavior of the Pd-based and Zr-based bulk metallic glasses. They found that it has much more serrations on load-displacement curves when loading rate is smaller, and vice versa. The decrease of loading rate can make more plastic deformation due to the serrations. When the loading rate is enhanced, lots of shear bands will work at the same time. This means that the plastic deformation can't sufficiently develop in specific shear band. It will induce the generation of smooth load- displacement curve. While as for alloy composition, it is well known that that activation of STZ is much more sensitive to local structural heterogeneities. Cao et al. [75] found that the distribution of load-displacement curves for softer La-based metallic

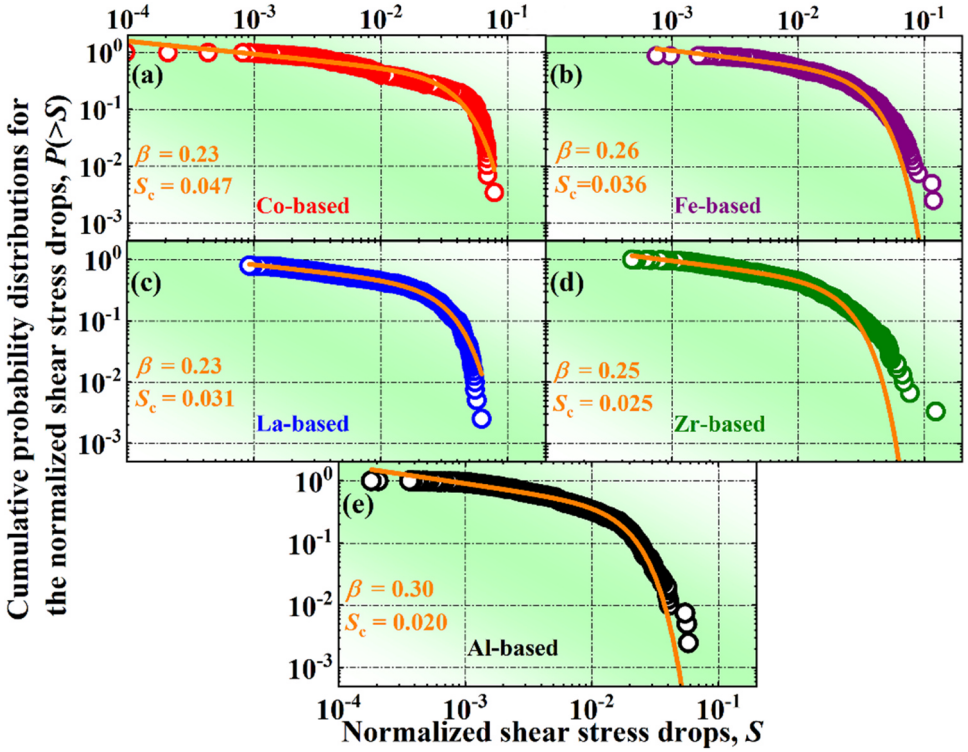

Fig. 6. Logarithmic plot of cumulative probability distributions of serration size for samples of Co, Fe, La, Zr, and Al-based MGs (a-e, respectively). Solid lines are fitting curves from Eq. 5.

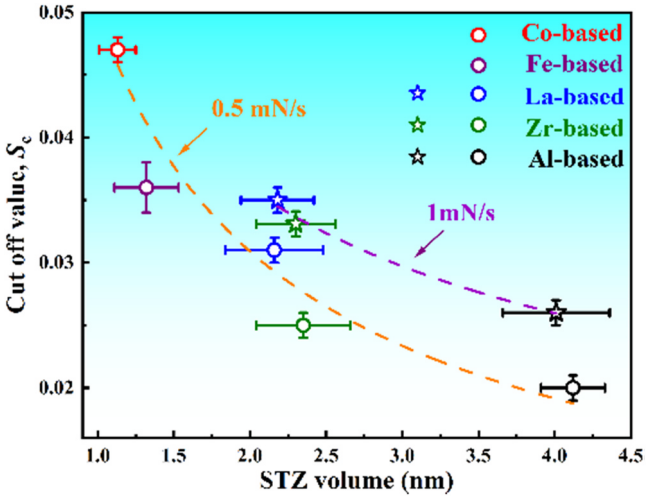

Fig. 7. Variation of the cutoff value with STZ volumes at loading rates of 0.5 and 1 mN/s.

glass is relatively wider as compared with Zr-based metallic glass, since it contains more structural heterogeneity sites. In addition, the effect of loading rate on these parameters is much weaker comparing with the effect of the metallic glass compositions.

5. Conclusions

The relationship between the STZ and serrated flow dynamics of Co-, Fe-, Zr-, La-, and Al-based MGs samples under nanoindentation testing with a standard Berkovich tip were theoretically and experimentally analyzed. In view of the above experimental observations and analysis, the following conclusions were drawn.

(1) The frequency and size of serrations on the τ-h curve were affected by the alloy composition and loading rate testing conditions. The serration flow phenomenon was more clear and serrated flow dynamics behavior observed in a SOC state at low loading rates. As the loading rate increased, the dynamic state of serration flow changed from the SOC to chaotic behavior, which first occurred in the hard Co and Fe-based MGs.

(2) Based on the CSM theory, the nanoindentation creep method was used to calculate the STZ volume. The loading rate effect on the STZ volume of the Co-based MG was weak. However, the STZ volume of other MGs exhibited a decreasing trend when the serrated flow dynamics behavior was in a chaotic state. Further, the STZ volume decreased markedly in soft MGs (i.e., Al- and Zr-based) and receded little in less-ductile MGs (i.e., La- and Fe-based).

(3) An ergodic processing was introduced to analyze the distribution of normalized shear stress drops. The cut off value, S_c, decreased with increased the STZ volumes, which reflected that the STZ activation facilitated SOC formation.

CRediT authorship contribution statement

I have made substantial contributions to the conception or design of the work or the acquisition, analysis, or interpretation of data for the work; AND I have drafted the work or revised it critically for important intellectual content; AND I have approved the final version to be published; AND I agree to be accountable for all aspects of the work in ensuring that questions related to the accuracy or integrity of any part of the work are appropriately investigated and resolved. All persons who have made substantial contributions to the work reported in the manuscript, including those who provided editing and writing assistance but who are not authors, are named in the Acknowledgments section of the manuscript and have given their written permission to be named. If the manuscript does not include Acknowledgments, it is because the authors have not received substantial contributions from nonauthors.

Data Availability

Data will be made available on request.

Declaration of Competing Interest

The authors declare that they have no known competing financial interests or personal relationships that could have appeared to influence the work reported in this paper.

Acknowledgments

The present work was supported by National Natural Science Foundation of China (52101037), Natural Science Foundation of Liaoning Province (2021-KF-15-01), The Grant Plan for Young and Middle-aged Innovation Scientists of Shenyang Government (RC210058) and Basic Scientific Research Project of Education Department of Liaoning Province (LJKMZ20220466). PKL very much appreciates the supports from the National Science Foundation (No. DMR-1611180 and 1809640).

References

[1] J.C. Qiao, Q. Wang, J.M. Pelletier, H. Kato, R. Casalini, D. Crespo, E. Pineda, Y. Yao, Y. Yang, Structural heterogeneities and mechanical behavior of amorphous alloys, Prog. Mater. Sci. 104 (2019) 250–329.
[2] Y.Q. Cheng, E. Ma, Atomic-level structure and structure–property relationship in metallic glasses, Prog. Mater. Sci. 56 (4) (2011) 379–473.
[3] M.F. Ashby, A.L. Greer, Metallic glasses as structural materials, Scr. Mater. 54 (3) (2006) 321–326.
[4] H.X. Li, Z.C. Lu, S.L. Wang, Y. Wu, Z.P. Lu, Fe-based bulk metallic glasses: glass formation, fabrication, properties and applications, Prog. Mater. Sci. 103 (2019) 235–318.
[5] M.M. Trexler, N.N. Thadhani, Mechanical properties of bulk metallic glasses, Prog. Mater. Sci. 55 (8) (2010) 759–839.
[6] C.A. Schuh, T.C. Hufnagel, U. Ramamurty, Mechanical behavior of amorphous alloys, Acta Mater. 55 (12) (2007) 4067–4109.
[7] B.A. Sun, W.H. Wang, The fracture of bulk metallic glasses, Prog. Mater. Sci. 74 (2015) 211–307.
[8] W.H. Wang, Dynamic relaxations and relaxation-property relationships in metallic glasses, Prog. Mater. Sci. 106 (2019) 100561.
[9] Y. Zhang, J.P. Liu, S.Y. Chen, X. Xie, P.K. Liaw, K.A. Dahmen, J.W. Qiao, Y.L. Wang, Serration and noise behaviors in materials, Prog. Mater. Sci. 90 (2017) 358–460.
[10] L. Zhang, Y. Duan, D. Crespo, E. Pineda, Y. Wang, J.-M. Pelletier, J. Qiao, Dynamic mechanical relaxation and thermal creep of high-entropy La30Ce30Ni10Al20Co10 bulk metallic glass, Sci. China Phys. Mech. Astron. 64 (9) (2021) 296111.
[11] F.Y. Dong, M.Y. He, Y. Zhang, B. Wang, L. Luo, Y. Su, H. Yang, X. Yuan, Investigation of shear transformation zone and ductility of Zr-based bulk metallic glass after plasma-assisted hydrogenation, Mater. Sci. Eng. A 759 (24) (2019) 105–111.
[12] J. Pan, F.H. Duan, Rejuvenation behaviors in metallic glasses, Acta Met. Sin. 57 (04) (2021).
[13] J. Pan, Y.X. Wang, Q. Guo, D. Zhang, A.L. Greer, Y. Li, Extreme rejuvenation and softening in a bulk metallic glass, Nat. Commun. 9 (1) (2018) 560.
[14] F. Spaepen, A microscopic mechanism for steady state inhomogeneous flow in metallic glasses, Acta Metall. 25 (4) (1977) 407–415.
[15] C.F. Ma, S. Li, P. Huang, F. Wang, Size dependent hidden serration behaviors of shear banding in metallic glass thin films, J. Non-Cryst. Solids 534 (2020) 119953.
[16] A.L. Greer, Y.Q. Cheng, E. Ma, Shear bands in metallic glasses, Mater. Sci. Eng. Rep. 74 (4) (2013) 71–132.
[17] A.L. Greer, A. Castellero, S.V. Madge, I.T. Walker, J.R. Wilde, Nanoindentation studies of shear banding in fully amorphous and partially devitrified metallic alloys, Mater. Sci. Eng.: A 375 (2004) 1182–1185.
[18] W.H. Jiang, F.X. Liu, P.K. Liaw, H. Choo, Shear strain in a shear band of a bulk-metallic glass in compression, Appl. Phys. Lett. 90 (18) (2007).
[19] J.W. Liu, Q.P. Cao, L.Y. Chen, X.D. Wang, J.Z. Jiang, Shear band evolution and hardness change in cold-rolled bulk metallic glasses, Acta Mater. 58 (14) (2010) 4827–4840.
[20] A.S. Argon, Plastic deformation in metallic glasses, Acta Metall. 27 (1) (1979) 47–58.
[21] K. Tao, J.C. Qiao, Q.F. He, K.K. Song, Y. Yang, Revealing the structural heterogeneity of metallic glass: mechanical spectroscopy and nanoindentation experiments, Int. J. Mech. Sci. 201 (2021) 106469.
[22] L. Tian, D. Tonnies, M. Hirsbrunner, T. Sievert, Z.W. Shan, C.A. Volkert, Effect of hydrogen charging on pop-in behavior of a Zr-based metallic glass, Metals 10 (1) (2020) 22.
[23] C.Y. Liu, R. Maass, Elastic fluctuations and structural heterogeneities in metallic glasses, Adv. Funct. Mater. 28 (30) (2018).
[24] X.L. Bian, D. Zhao, J.T. Kim, D. Sopu, G. Wang, R. Pippan, J. Eckert, Controlling the distribution of structural heterogeneities in severely deformed metallic glass, Mater. Sci. Eng. a Struct. Mater. Prop. Microstruct. Process. 752 (2019) 36–42.
[25] F.Y. Dong, Y.X. Chu, M. He, Y. Zhang, W. Li, P.K. Liaw, B. Wang, L. Luo, Y. Su, R.O. Ritchie, X. Yuan, Manipulating internal flow units toward favorable plasticity in Zr-based bulk-metallic glasses by hydrogenation, J. Mater. Sci. Technol. 102 (2022) 36–45.
[26] F. Zhu, A. Hirata, P. Liu, S. Song, Y. Tian, J. Han, T. Fujita, M. Chen, Correlation between local structure order and spatial heterogeneity in a metallic glass, Phys. Rev. Lett. 119 (21) (2017) 215501.
[27] Z. Wang, J.W. Qiao, H. Tian, B.A. Sun, B.C. Wang, B.S. Xu, M.W. Chen, Composition mediated serration dynamics in Zr-based bulk metallic glasses, Appl. Phys. Lett. 107 (20) (2015).
[28] N.P. Bailey, J. Schiøtz, A. Lemaître, K.W. Jacobsen, Avalanche size scaling in sheared three-dimensional amorphous solid, Phys. Rev. Lett. 98 (9) (2007) 095501.
[29] J.W. Qiao, Y. Zhang, P.K. Liaw, Serrated flow kinetics in a Zr-based bulk metallic glass, Intermetallics 18 (11) (2010) 2057–2064.
[30] R. Sarmah, G. Ananthakrishna, B.A. Sun, W.H. Wang, Hidden order in serrated flow of metallic glasses, Acta Mater. 59 (11) (2011) 4482–4493.
[31] L.T. Zhang, Y.J. Duan, T. Wada, H. Kato, J.M. Pelletier, D. Crespo, E. Pineda, J.C. Qiao, Dynamic mechanical relaxation behavior of $Zr_{35}Hf_{17.5}Ti_{5.5}Al_{12.5}Co_{7.5}Ni_{12}Cu_{10}$ high entropy bulk metallic glass, J. Mater. Sci. Technol. 83 (2021) 248–255.
[32] D. Pan, Y. Yokoyama, T. Fujita, Y.H. Liu, S. Kohara, A. Inoue, M.W. Chen, Correlation between structural relaxation and shear transformation zone volume of a bulk metallic glass, Appl. Phys. Lett. 95 (14) (2009).
[33] B.S. Shang, P.F. Guan, J.L. Barrat, Elastic avalanches reveal marginal behavior in amorphous solids, Proc. Natl. Acad. Sci. USA 117 (1) (2020) 86–92.
[34] X.L. Bian, G. Wang, K.C. Chan, J.L. Ren, Y.L. Gao, Q.J. Zhai, Shear avalanches in metallic glasses under nanoindentation: deformation units and rate dependent strain burst cut-off, Appl. Phys. Lett. 103 (10) (2013) 101907.
[35] J.J. Li, J.W. Qiao, Y.C. Wu, Seismic-like size dynamics of slip avalanches in bulk metallic glasses, J. Alloy. Compd. 819 (2020) 152941.
[36] B.A. Sun, H.B. Yu, W. Jiao, H.Y. Bai, D.Q. Zhao, W.H. Wang, Plasticity of ductile metallic glasses: a self-organized critical state, Phys. Rev. Lett. 105 (3) (2010) 035501.
[37] M.S. Bharathi, M. Lebyodkin, G. Ananthakrishna, C. Fressengeas, L.P. Kubin, Multifractal burst in the spatiotemporal dynamics of jerky flow, Phys. Rev. Lett. 87 (16) (2001) 165508.
[38] J.O. Krisponeit, S. Pitikaris, K.E. Avila, S. Kuchemann, A. Kruger, K. Samwer, Crossover from random three-dimensional avalanches to correlated nano shear bands in metallic glasses, Nat. Commun. 5 (2014) 3616.
[39] K.P. Marimuthu, K. Lee, J. Han, F. Rickhey, H. Lee, Nanoindentation of zirconium based bulk metallic glass and its nanomechanical properties, J. Mater. Res. Technol. 9 (1) (2020) 104–114.
[40] C.A. Schuh, A.S. Argon, T.G. Nieh, J. Wadsworth, The transition from localized to homogeneous plasticity during nanoindentation of an amorphous metal, Philos. Mag. 83 (22) (2003) 2585–2597.
[41] C.A. Schuh, A.C. Lund, T.G. Nieh, New regime of homogeneous flow in the deformation map of metallic glasses: elevated temperature nanoindentation experiments and mechanistic modeling, Acta Mater. 52 (20) (2004) 5879–5891.
[42] W.L. Johnson, K. Samwer, A universal criterion for plastic yielding of metallic glasses with a $(T/T_g)^{2/3}$ temperature dependence, Phys. Rev. Lett. 95 (19) (2005) 195501.
[43] Y. Ma, G.J. Peng, T.T. Debela, T.H. Zhang, Nanoindentation study on the characteristic of shear transformation zone volume in metallic glassy films, Scr. Mater. 108 (2015) 52–55.
[44] G.K. Liao, Z.L. Long, M.S.Z. Zhao, L. Peng, W. Chai, Z.H. Ping, Nanoindentation study on the characteristic of shear transformation zone in a Pd-based bulk metallic glass during serrated flow, Phys. B Condens. Matter 534 (2018) 163–168.
[45] I.C. Choi, Y. Zhao, Y.J. Kim, B.G. Yoo, J.Y. Suh, U. Ramamurty, Ji Jang, Indentation size effect and shear transformation zone size in a bulk metallic glass in two different structural states, Acta Mater. 60 (19) (2012) 6862–6868.
[46] V. Maier, B. Merle, M. Göken, K. Durst, An improved long-term nanoindentation creep testing approach for studying the local deformation processes in nanocrystalline metals at room and elevated temperatures, J. Mater. Res. 28 (9) (2013) 1177–1188.
[47] A.C. Fischer-Cripps, A simple phenomenological approach to nanoindentation creep, Mater. Sci. Eng. A 385 (1) (2004) 74–82.
[48] B.C. Wei, L.C. Zhang, T.H. Zhang, D.M. Xing, J. Das, J. Eckert, Strain rate dependence of plastic flow in Ce-based bulk metallic glass during nanoindentation, J. Mater. Res. 22 (2) (2007) 258–263.
[49] H.C. Sun, Z.L. Ning, J.L. Ren, W.Z. Liang, Y.J. Huang, J.F. Sun, X. Xue, G. Wang, Serration and shear avalanches in a ZrCu based bulk metallic glass composite in different loading methods, J. Mater. Sci. Technol. 35 (9) (2019) 2079–2085.
[50] C. Schuh, T.G. Nieh, A survey of instrumented indentation studies on metallic glasses, J. Mater. Res. 19 (1) (2004) 46–57.
[51] W.C. Oliver, G.M. Pharr, An improved technique for determining hardness and elastic modulus using load and displacement sensing indentation experiments, J. Mater. Res. 7 (6) (1992) 1564–1583.
[52] I.C. Choi, Y. Zhao, B.G. Yoo, Y.J. Kim, J.Y. Suh, U. Ramamurty, Ji Jang, Estimation of the shear transformation zone size in a bulk metallic glass through statistical analysis of the first pop-in stresses during spherical nanoindentation, Scr. Mater. 66 (11) (2012) 923–926.

[53] T.G. Nieh, C. Schuh, J. Wadsworth, Y. Li, Strain rate-dependent deformation in bulk metallic glasses, Intermetallics 10 (11–12) (2002) 1177–1182.
[54] Q.L. Chu, S. Xu, X.F. Zhu, Z.W. Zhu, H.F. Zhang, R.X. Bai, Z.K. Lei, C. Yan, Effects of testing conditions on the deformation behaviour of a Ti-based bulk metallic glass, Mater. Sci. Eng. a Struct. Mater. Prop. Microstruct. Process. 766 (2019).
[55] C.A. Schuh, T.G. Nieh, Y. Kawamura, Rate dependence of serrated flow during nanoindentation of a bulk metallic glass, J. Mater. Res. 17 (7) (2002) 1651–1654.
[56] Y.M. Lu, B.A. Sun, L.Z. Zhao, W.H. Wang, M.X. Pan, C.T. Liu, Y. Yang, Shear-banding induced indentation size effect in metallic glasses, Sci. Rep. 6 (2016) 28523.
[57] J.I. Jang, B.G. Yoo, Y.J. Kim, J.H. Oh, I.C. Choi, H.B. Bei, Indentation size effect in bulk metallic glass, Scr. Mater. 64 (8) (2011) 753–756.
[58] H. Li, A.H.W. Ngan, M.G. Wang, Continuous strain bursts in crystalline and amorphous metals during plastic deformation by nanoindentation, J. Mater. Res. 20 (11) (2005) 3072–3081.
[59] B.A. Sun, S. Pauly, J. Tan, M. Stoica, W.H. Wang, U. Kühn, J. Eckert, Serrated flow and stick-slip deformation dynamics in the presence of shear-band interactions for a Zr-based metallic glass, Acta Mater. 60 (10) (2012) 4160–4171.
[60] J. Hu, B.A. Sun, Y. Yang, C.T. Liu, S. Pauly, Y.X. Weng, J. Eckert, Intrinsic versus extrinsic effects on serrated flow of bulk metallic glasses, Intermetallics 66 (2015) 31–39.
[61] B. Yang, T.G. Nieh, Effect of the nanoindentation rate on the shear band formation in an Au-based bulk metallic glass, Acta Mater. 55 (1) (2007) 295–300.
[62] C. Zhong, H. Zhang, Q.P. Cao, X.D. Wang, D.X. Zhang, U. Ramamurty, J.Z. Jiang, Deformation behavior of metallic glasses with shear band like atomic structure: a molecular dynamics study, Sci. Rep. 6 (1) (2016) 30935.
[63] Y.Q. Cheng, E. Ma, Atomic-level structure and structure-property relationship in metallic glasses, Prog. Mater. Sci. 56 (4) (2011) 379–473.
[64] C. Maloney, A. Lemaitre, Universal breakdown of elasticity at the onset of material failure, Phys. Rev. Lett. 93 (19) (2004).
[65] F. Delogu, Molecular dynamics of shear transformation zones in metallic glasses, Intermetallics 16 (5) (2008) 658–661.
[66] F. Delogu, Identification and characterization of potential shear transformation zones in metallic glasses, Phys. Rev. Lett. 100 (2008) 255901.
[67] S. Mayr, Activation energy of shear transformation zones: a key for understanding rheology of glasses and liquids, Phys. Rev. Lett. 97 (19) (2006) 195501.
[68] Y. Fan, T. Iwashita, T. Egami, How thermally activated deformation starts in metallic glass, Nat. Commun. 5 (1) (2014) 5083.
[69] D. Pan, A. Inoue, T. Sakurai, M.W. Chen, Experimental characterization of shear transformation zones for plastic flow of bulk metallic glasses, Proc. Natl. Acad. Sci. 105 (39) (2008) 14769.
[70] D. Pan, Y. Yokoyama, T. Fujita, Y. Liu, S. Kohara, A. Inoue, M. Chen, Correlation between structural relaxation and shear transformation zone volume of a bulk metallic glass, Appl. Phys. Lett. 95 (2009) 141909.
[71] Y. Ma, J.H. Ye, G.J. Peng, D.H. Wen, T.H. Zhang, Nanoindentation study of size effect on shear transformation zone size in a Ni–Nb metallic glass, Mater. Sci. Eng.: A 627 (2015) 153–160.
[72] P. Bak, C. Tang, K. Wiesenfeld, Self-organized criticality: an explanation of the 1/f noise, Phys. Rev. Lett. 59 (4) (1987) 381–384.
[73] Z. Budrikis, S. Zapperi, Avalanche localization and crossover scaling in amorphous plasticity, Phys. Rev. E 88 (6) (2013) 062403.
[74] G. Wang, N. Mattern, J. Bednarčík, R. Li, B. Zhang, J. Eckert, Correlation between elastic structural behavior and yield strength of metallic glasses, Acta Mater. 60 (6) (2012) 3074–3083.
[75] Q.P. Cao, L.J. Sun, C. Wang, Y. Fu, S.Y. Liu, S.X. Qu, X.D. Wang, D.X. Zhang, J.Z. Jiang, Effect of loading rate on creep behavior and shear transformation zone in amorphous alloy thin fifilms, and its correlation with deformation mode transition, Thin Solid Films 681 (2019) 23–31.